



Contents lists available at ScienceDirect

Journal of the European Ceramic Society

journal homepage: [www.elsevier.com/locate/jeurceramsoc](http://www.elsevier.com/locate/jeurceramsoc)

## Drastic enhancement of mechanical properties of $\text{Ca}_3\text{Co}_4\text{O}_9$ by $\text{B}_4\text{C}$ addition

Hippolyte Amaveda<sup>a</sup>, Mario Mora<sup>a</sup>, Oscar J. Dura<sup>b</sup>, Miguel A. Torres<sup>a</sup>, Maria A. Madre<sup>a</sup>, Sylvain Marinel<sup>c</sup>, Andres Sotelo<sup>a,\*</sup>

<sup>a</sup> ICMA (Universidad de Zaragoza-CSIC), Dpto. de Ciencia y Tecnología de Materiales y Fluidos, C/María de Luna 3, E-50018, Zaragoza, Spain

<sup>b</sup> Departamento de Física Aplicada, Universidad de Castilla-La Mancha, E-13071 Ciudad, Real, Spain

<sup>c</sup> Normandie Univ, ENSICAEN, UNICAEN, CNRS, CRISMAT, 14000 Caen, France

### ARTICLE INFO

#### Keywords:

Ceramics  
Oxides  
Mechanical properties  
Thermoelectric properties  
Thermal expansion

### ABSTRACT

$\text{Ca}_3\text{Co}_4\text{O}_9$  with  $\text{B}_4\text{C}$  additions in different proportions (0, 0.10, 0.25, 0.5, and 0.75 wt.%) have been fabricated using the classical solid-state method. Powder XRD patterns have displayed that  $\text{Ca}_3\text{Co}_4\text{O}_9$  phase is the major one in all samples. Microstructural observations showed that  $\text{B}_4\text{C}$  has been superficially oxidized, producing liquid  $\text{B}_2\text{O}_3$  during sintering, and reacting with the  $\text{Ca}_3\text{Co}_4\text{O}_9$  grains to produce bridges between them. In spite of the increase of porosity, these bridges led to an important raise (more than two times) of mechanical properties when compared to the pristine materials. On the other hand, while  $\text{B}_4\text{C}$  addition has not influenced  $S$  values, it has decreased electrical resistivity, thermal conductivity, and thermal expansion. Consequently,  $ZT$  values have been also increased, reaching 0.24 at 800 °C in 0.25 wt.%  $\text{B}_4\text{C}$  containing samples, which is very close to the best values reported in the literature, and two times higher than the obtained in pure materials in this work.

### 1. Introduction

Thermoelectric (TE) technology is considered as a very promising one to enhance energy transforming devices efficiency by harvesting wasted heat [1]. This characteristic is associated to the Seebeck effect, which is inherent to the TE materials [2]. On the other hand, these materials should display appropriate thermoelectric properties for practical applications, evaluated using the equation [3]:

$$ZT = \frac{S^2 T \sigma}{\kappa} \quad (1)$$

where  $ZT$  is the dimensionless Figure-of-Merit, and  $S$ ,  $T$ ,  $\sigma$ , and  $\kappa$  are Seebeck coefficient, absolute temperature, and electrical, and thermal conductivity, respectively.

TE materials are considered adequate for practical applications when their  $ZT$  values are higher than 1. Nowadays, only intermetallic materials display these values at low-medium temperatures [4,5], with the drawback of their usual chemical composition, comprising heavy elements. Moreover, they cannot be used at high temperatures due to oxidation processes, unless they are sealed to avoid oxidant environments. On the other hand, oxide materials possess high chemical and thermal stability, and can work at high temperatures. Moreover, they are composed of abundant, cheaper, and environmentally friendly elements [6]. However, their TE performances are lower than those

determined in intermetallic materials. Consequently, most of the works published in this field are dealing with the improvement of their TE performances through many different ways [7–13].

Nevertheless, TE properties of materials are not the only parameters determining the efficiency of a TE module. One of them is the so-called manufacturing factor (MF) which is a function of the ideal resistance in the module ( $R_{id}$ , taking into account the resistance of legs), and the real internal resistance ( $R_{int}$ , where the contact resistance is also present), as  $MF = R_{id}/R_{int}$  [14]. This MF is usually determined in the as-fabricated modules, but it can be decreased during the working life of these modules due to the differential expansion of the different components ( $p$ , and  $n$  thermoelectric legs, metallic parts, and insulating ceramic) which can damage the contacts among them, increasing the internal resistance. Consequently, before building a TE module, it is very convenient choosing materials with very close thermal expansion coefficients to avoid internal stresses when working at high temperature. Besides, high mechanical properties are also desired in these TE legs in order to maintain the module integrity and increasing its useful life.

In this work,  $\text{Ca}_3\text{Co}_4\text{O}_9$  material will be prepared, with the addition of small amounts of  $\text{B}_4\text{C}$  (0, 0.10, 0.25, 0.50, and 0.75 wt.%), via the classical solid-state route. The effect of these additions on the structure and microstructure of  $\text{Ca}_3\text{Co}_4\text{O}_9$  sintered pellets will be studied and related to the modifications produced in parameters such as linear expansion coefficient, mechanical, and thermoelectric properties.

\* Corresponding author at: C/María de Luna, 3, E-50018 Zaragoza, Spain.

E-mail address: [asotelo@unizar.es](mailto:asotelo@unizar.es) (A. Sotelo).

<https://doi.org/10.1016/j.jeurceramsoc.2020.08.024>

Received 24 June 2020; Received in revised form 8 August 2020; Accepted 11 August 2020

0955-2219/ © 2020 Elsevier Ltd. All rights reserved.

## 2. Experimental

$\text{Ca}_3\text{Co}_4\text{O}_9 + x \text{ wt.}\% \text{ B}_4\text{C}$ , with  $x = 0.0, 0.10, 0.25, 0.50,$  and  $0.75$ , have been prepared using the classical solid-state route from  $\text{CaCO}_3$  (Panreac, 98 + %), and  $\text{Co}_2\text{O}_3$  (Aldrich, 98 + %) commercial powders. They were weighed in the adequate amounts, mixed and ball milled under water media for 30 min at 300 rpm to produce a suspension, which was dried under infrared radiation. The resulting dry mixture was manually milled to produce a very fine powder, subsequently thermally treated at 750 and 800 °C for 12 h under air, with an intermediate manual milling. This thermal process is adequate to decompose  $\text{CaCO}_3$  and to produce intermediate by-products, in agreement with previously reported data [15]. After milling these calcined powders,  $\text{B}_4\text{C}$  (Alfa Aesar, 99 + %) has been added in the stoichiometric proportions and the mixture has been ball milled 30 min at 300 rpm to homogenize the mixture. After this process, the different materials were cold-pressed in form of pellets with around  $3 \times 3 \times 12 \text{ mm}^3$ , under 400 MPa applied pressure perpendicular to the  $3 \times 12 \text{ mm}^2$  surface. Finally, the compacts were sintered at 900 °C for 24 h under air atmosphere, followed by a final furnace cooling.

Powder X-ray diffraction (XRD) patterns were determined in a theta-theta PANalytical X'Pert Pro diffractometer ( $\text{CuK}\alpha$  radiation,  $\lambda = 1.54059 \text{ \AA}$ ) between 10 and 40 degrees, where the main peaks of  $\text{Ca}_3\text{Co}_4\text{O}_9$  phase, and the most intense of  $\text{B}_4\text{C}$ , appear. Density measurements were performed using Archimedes' method on several samples for each  $\text{B}_4\text{C}$  addition. The relative density values were calculated with respect to the theoretical one, assuming a dense and perfect mixture of  $\text{Ca}_3\text{Co}_4\text{O}_9$  ( $4.677 \text{ g/cm}^3$  [16]) and  $\text{B}_4\text{C}$  ( $2.50 \text{ g/cm}^3$  [17]).

Microstructural observations have been performed on the samples surfaces and fractured sections in a Field Emission Scanning Electron Microscope (FESEM, Carl Zeiss Merlin) combined with an energy-dispersive spectrometry (EDS) system. Mechanical properties have been determined in several samples for each composition through flexural strength, Young's modulus, compression tests and Vickers microhardness measurements. Flexural strength and Young's modulus have been obtained from the three point bending test in an Instron 5565, with  $30 \mu\text{m/s}$  punch displacement and 10 mm span; compressive strength was performed parallel to the long pellet axis at  $30 \mu\text{m/s}$ ; and Vickers microindentation tests were accomplished under 0.05 Kg applied load. Seebeck coefficient and electrical resistivity were simultaneously determined through the four-point contact, along the large pellet axis, using a LSR-3 (Linseis GmbH) under He atmosphere in the 50–800 °C temperature range. Thermal diffusivity ( $\alpha$ ) has been measured in the same direction used for the electrical characterization in a laser-flash system (Linseis LFA 1000). Thermal conductivity ( $\kappa$ ) has been calculated as  $\kappa = \alpha C_p d$ , being  $C_p$  specific heat and  $d$ , sample density.  $C_p$  has been determined through Dulong-Petit law. From  $d$ ,  $C_p$ ,  $E$ , and  $\kappa$ , phonon mean free path has been calculated for each composition. In order to establish the samples TE performances, ZT was determined from Seebeck coefficient, electrical resistivity, and thermal conductivity data. These data were used to evaluate the properties evolution as a function of the dopant content, and were also compared with previously reported values in the literature for similar compounds. Finally, dilatometric behaviour of samples has been studied in the 25–800 °C temperature range in a L79 HCS dilatometer (Linseis GmbH) to determine their linear expansion coefficient evolution as a function of  $\text{B}_4\text{C}$  content.

## 3. Results and discussion

### 3.1. Structural and microstructural characterization

Fig. 1 illustrates the XRD patterns obtained in  $\text{Ca}_3\text{Co}_4\text{O}_9 + x \text{ wt.}\% \text{ B}_4\text{C}$  powdered samples. As it can be easily observed in the figure, all samples present very similar patterns, independently of the  $\text{B}_4\text{C}$  addition. Moreover, all peaks can be associated to the diffraction planes

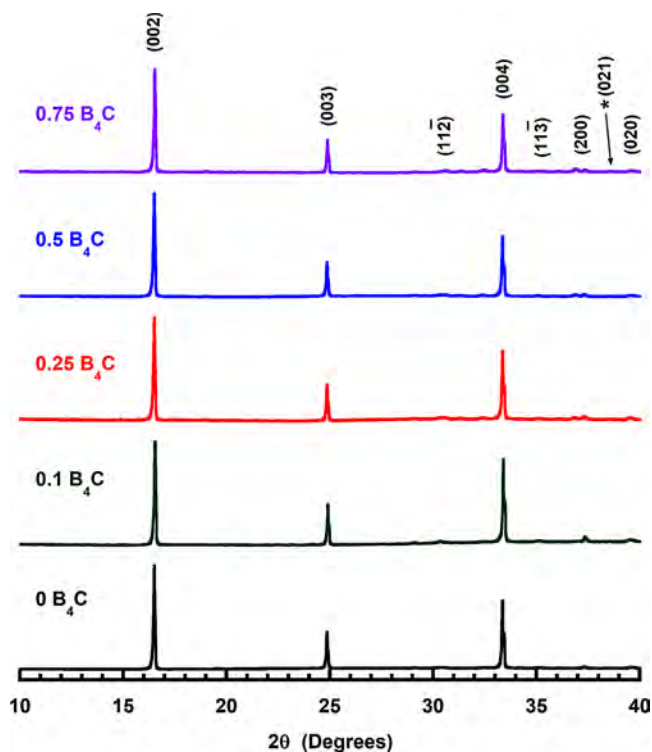


Fig. 1. Powder X-ray diffraction patterns of  $\text{Ca}_3\text{Co}_4\text{O}_9 + x \text{ wt.}\% \text{ B}_4\text{C}$  samples. The diffraction planes indicate the reflections of  $\text{Ca}_3\text{Co}_4\text{O}_9$  phase. \* identifies the  $\text{B}_4\text{C}$  diffraction peak.

(indicated in the graph) of  $\text{Ca}_3\text{Co}_4\text{O}_9$  phase with monoclinic symmetry [18,19]. Furthermore, the most intense diffractions correspond to its  $ab$ -planes, which could be associated to preferential grain orientation. However, it should be highlighted that XRD patterns were obtained on powdered samples and, consequently, this grain orientation is produced by the samples preparation, as observed in previous works [20]. On the other hand,  $\text{B}_4\text{C}$  has been identified with this technique through its (021) reflection peak at 37.818 degrees, appearing with very low intensity for  $\text{B}_4\text{C}$  content  $\geq 0.25 \text{ wt.}\%$  [21].

Microstructural studies performed on the samples surfaces have shown that all samples are composed of flake-like particles with no preferential orientation, which is the characteristic situation in this system, as reported in previous works [22,23]. Moreover, EDS analysis has confirmed the XRD results, showing that these grains correspond to the  $\text{Ca}_3\text{Co}_4\text{O}_9$  phase. On the other hand, the  $\text{Ca}_3\text{Co}_4\text{O}_9$  grain sizes are decreased when the amount of  $\text{B}_4\text{C}$  is increased, while porosity seems to be increased. In order to confirm the raise in porosity when the  $\text{B}_4\text{C}$  content is larger, the samples density was evaluated and the mean results, together with their standard error, are displayed in Table 1. As it is clear from these data, samples density is slightly decreased when the amount of  $\text{B}_4\text{C}$  is increased, corroborating the SEM observations. In any case, the relative density values are in the order of the typically reported in materials prepared through the classical solid-state method [23–25]. This low densification can be explained when considering the

Table 1  
Apparent density, standard error, and relative density determined through Archimedes' method.

$\text{B}_4\text{C}$ content (wt.%)	Density ( $\text{g/cm}^3$ )	Std. error	Relative density
0	3.4532	0.0317	73.8
0.10	3.4358	0.0830	73.6
0.25	3.3742	0.0627	72.3
0.5	3.3205	0.0289	71.3
0.75	3.3009	0.0502	71.0

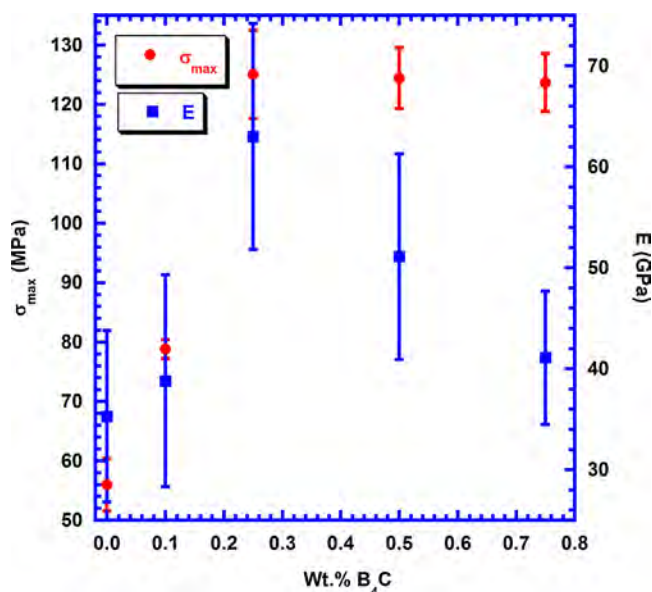


Fig. 2.  $\sigma_{\max}$  and E values obtained through three point bending tests, with their standard error, as a function of  $B_4C$  content.

phase equilibria diagram [26], which shows that  $Ca_3Co_4O_9$  phase is stable up to 926 °C. Consequently, sintering procedure has to be performed below this temperature, which is, in turn, much lower than the eutectic temperature (1350 °C), drastically limiting the samples densification. Even if porosity is undesirable to get very high mechanical properties, it can help reducing thermal conductivity of these samples and, consequently, increasing thermoelectric performances.

### 3.2. Mechanical characterization

Fig. 2 presents the three point bending tests results for the  $Ca_3Co_4O_9$  and their standard errors, together with the Young's modulus values extracted for these tests, as a function of  $B_4C$  content. In spite of the slight decrease of density induced by  $B_4C$  addition, mechanical properties are drastically increased, when compared to the pure samples. Flexural strength is increased in around 50 % for 0.1 wt.%  $B_4C$  addition, and more than 100 % for higher contents, while Young's modulus is only raised in around 10 % for 0.1 wt.%  $B_4C$  addition, and about 75 % for 0.25 wt.%  $B_4C$  samples. These results seem to be contradictory with the porosity evolution and, consequently, the fractured sections of samples were microstructurally studied.

Fig. 3 shows representative micrographs at high magnification of 0.25, and 0.75  $B_4C$  samples. As it can be observed in the pictures, besides the grey contrast ( $Ca_3Co_4O_9$  phase), a new contrast (dark grey) is appearing in higher proportions when the amount of  $B_4C$  is increased, which is connecting thermoelectric grains. EDS analysis has shown that this contrast contains B, C, O, Ca, and Co. These cations are present in a relationship (using B as reference)  $1.0:0.485 \pm 0.005:2.85 \pm 0.09:0.77 \pm 0.02:0.66 \pm 0.04$ , for B, C, O, Ca, and Co, respectively, independently of  $B_4C$  content. The formation of this new phase can be explained when considering that  $B_4C$  starts to be oxidized under air at around 450 °C, producing  $CO_2$  and  $B_2O_3$  [27]. This effect could lead to the total  $B_4C$  oxidation, however, the formed  $B_2O_3$  has melting point of 450 °C [28] and, between 600 and 1000 °C, forms a protective layer on the particles surface avoiding further oxidation [29]. On the other hand, the presence of this liquid phase, making close contact with the thermoelectric grains, lead to Ca-B-O [30], and Co-B-O [31] compounds formation on the  $B_4C$  particles surface. Consequently, these compounds form bridges between the thermoelectric grains, enhancing the samples mechanical properties. Bending stresses obtained in pure samples (56 MPa) are more than three times higher than the reported

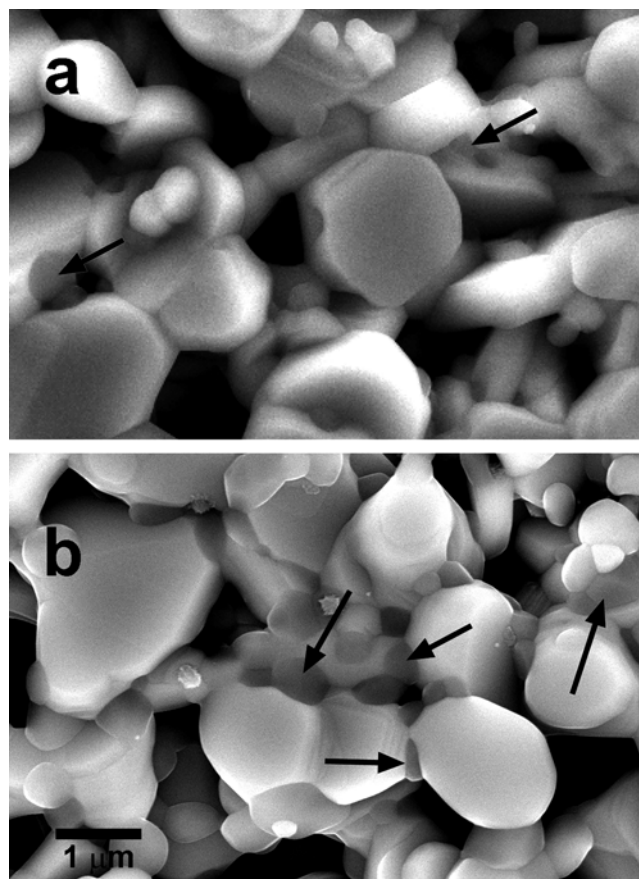


Fig. 3. Representative SEM micrographs obtained in fractured surfaces of  $Ca_3Co_4O_9 + x$  wt.%  $B_4C$ , with  $x = a)$  0.25; and  $b)$  0.75. The arrows show the dark grey contrast which corresponds to a B-rich phase.

for sintered samples (18.4 MPa) [32]. However, despite the adverse porosity effect, the best bending stress values were obtained in samples with  $B_4C$  content  $\geq 0.25$  wt.% (125 MPa). These values are about a half of the reported for high density materials with well oriented grains (254 MPa) [32]. Moreover, Young's modulus determined in 0.25 wt.%  $B_4C$  samples is only 35 % lower than the best reported values in this kind of materials [32].

Fig. 4 displays compressive strength of the different samples, as a function of  $B_4C$  content. As it is expected, the stresses determined through this test are higher than the obtained through three point bending tests. The evolution illustrated in the graph clearly confirms the effect of  $B_4C$  addition observed in the three point bending tests. In spite of the slight increase of samples porosity when  $B_4C$  is added, compressive strength is drastically increased by a factor 2 for  $B_4C$  content  $\geq 0.25$  wt.%, when compared to the pristine samples prepared in this work. On the other hand, slight differences with the three point bending test can be found in the graph, as stresses obtained by compression are asymptotically increased when  $B_4C$  content is higher than 0.25 wt.%.

Other important mechanical characteristic is the material hardness, which is responsible for the machinability and wear resistance of individual thermoelectric elements [32–34]. This property has been determined through Vickers microhardness, and the obtained results are presented, together with their standard error, in Fig. 5, as a function of  $B_4C$  content. As it can be seen in the graph, in spite of the porosity influence on the measurements, a clear increase of microhardness with the  $B_4C$  amount is produced. This evolution is in agreement with the microstructural features already discussed in Fig. 3, which enhance all mechanical properties determined in this work. Moreover, the values for the pristine samples (0.11 GPa) are the same reported in previous

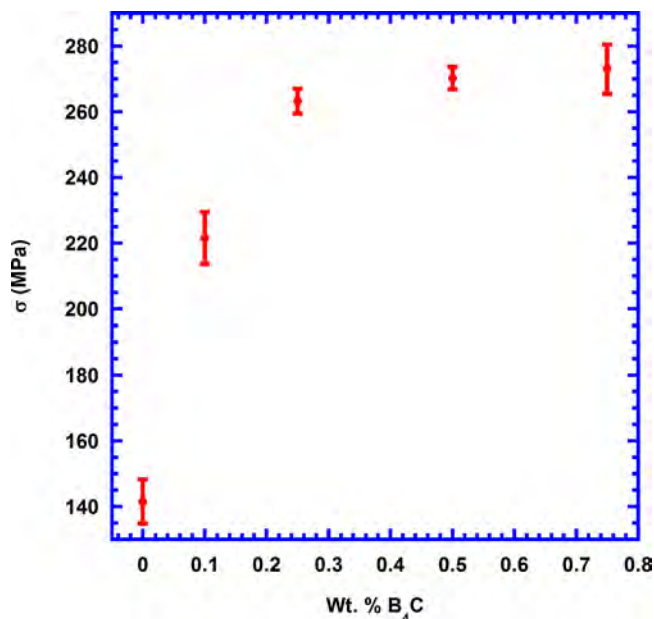


Fig. 4.  $\sigma$  values obtained through compression tests, with their standard error, as a function of  $B_4C$  content.

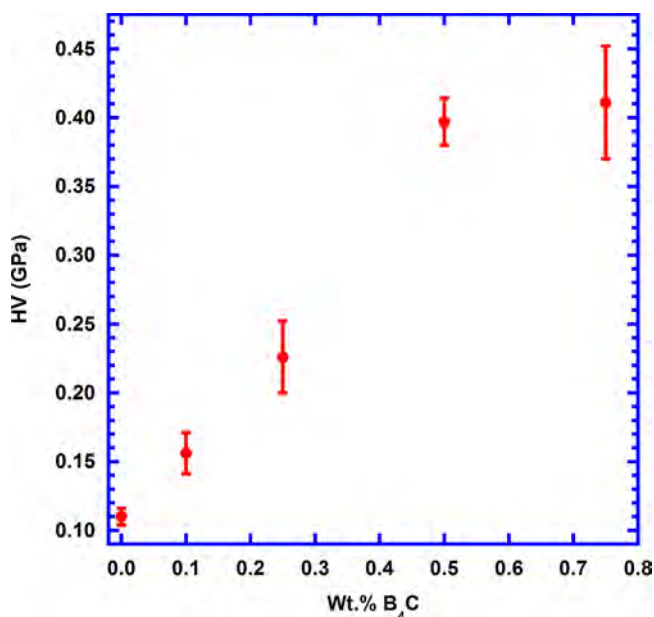


Fig. 5. Vickers microhardness values, with their standard error, as a function of  $B_4C$  addition.

works (0.12 GPa) [32], while the best results in samples with  $B_4C$  addition (0.41 GPa) can reach one third of the reported for nearly fully dense materials (1.3 GPa after hot pressing at 30 MPa) [32].

It is important to highlight that these porous samples with  $B_4C$  addition reach much higher mechanical properties than the expected in this kind of materials, not very far from the obtained in nearly fully dense materials, but using a more simple, economic, and rapid process. This is a very advantageous situation when considering these materials for practical applications.

### 3.3. Thermoelectric characterization

Electrical resistivity variation with temperature, as a function of  $B_4C$  content is presented in Fig. 6. As shown in the plot, all samples possess

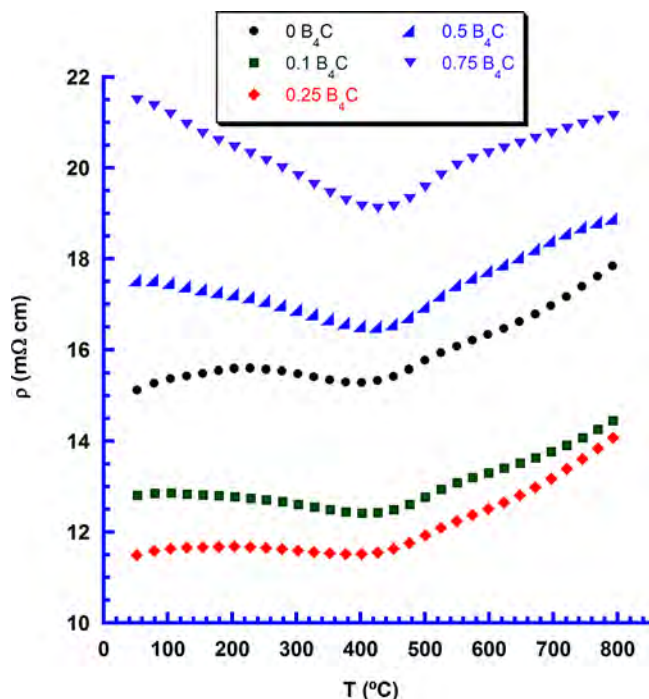


Fig. 6. Electrical resistivity variation with temperature, as a function of  $B_4C$  content, in  $Ca_3Co_4O_9 + x$  wt.%  $B_4C$  samples.

very similar behaviour in the whole measured temperature range. The samples display a minimum at around 450 °C, which corresponds to the change between semiconducting ( $d\rho/dT < 0$ ) and metallic ( $d\rho/dT > 0$ ) behaviour. This temperature indicates the change from a hole hopping from  $Co^{4+}$  to  $Co^{3+}$  [35] to a charge carriers transport in the valence or conduction band [36]. This is a very common behaviour observed in  $Ca_3Co_4O_9$  sintered materials [23,37]. On the other hand,  $B_4C$  addition up to 0.25 wt.% decreases electrical resistivity, while further addition drastically increases it, when compared to samples without additions. Different assumptions can be made to account for this. It can be due to a chemical effect such as the one already observed in CCO thin films, where a slightly lower Co content, with respect to the stoichiometric one, leads to lower electrical resistivity [38]. The latter mechanism may explain the decrease of the electrical resistivity of CCO, for the lowest  $B_4C$  addition, as this addition induces a slight departure of cobalt from the structure. However, other phenomena may be considered such as those related to the microstructure changes (grain size modification with  $B_4C$  addition, inter-granular insulating phase formation, etc.). It is clear that further investigations would be required to address this issue in detail. The lowest electrical resistivity values have been obtained in samples with 0.25 wt.%  $B_4C$ . The minimum resistivity values measured in these samples at 800 °C (14 mΩ cm) are slightly lower than the best values reported for  $Ca_3Co_4O_9$  samples sintered or textured through spark plasma sintering (15–18 mΩ cm) [39] and around 20 % lower than in pure samples. However, they are higher than the measured in highly dense materials prepared using alternative methods (10 mΩ cm) [40].

Fig. 7 shows the  $S$  variation with temperature and  $B_4C$  content.  $S$  displays positive values in all samples, indicating that conduction is mainly produced by holes. Moreover, the behaviour is the same for all samples, the values are increased when the temperature rises, and these values are the same for all samples within the measurement errors. These very close  $S$  values, independently of  $B_4C$  content can be explained by the very small compositional modification produced in the samples discussed previously. Furthermore, the cations drainage induced by the liquid  $B_2O_3$  is probably limited to the zones close to the grain boundaries, maintaining the core of the grains practically

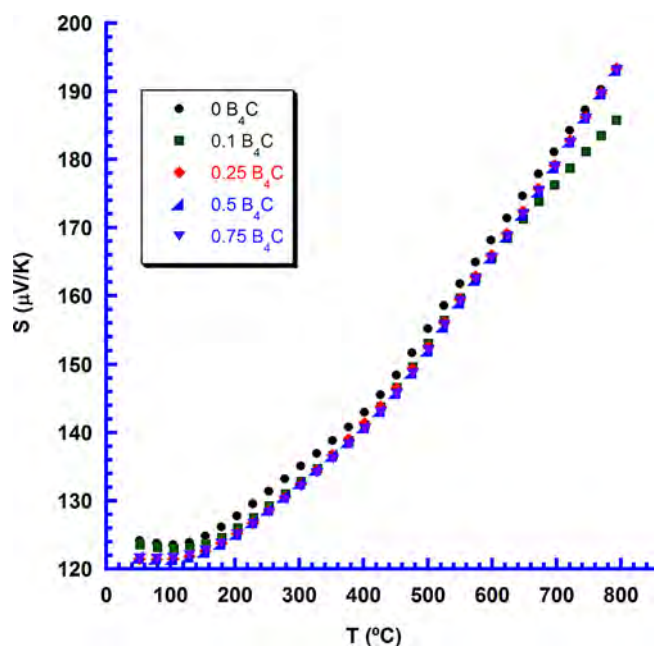


Fig. 7. Seebeck coefficient variation with temperature, as a function of  $B_4C$  content, in  $Ca_3Co_4O_9 + x$  wt.%  $B_4C$  samples.

unchanged. Consequently, no significant modifications in  $S$  values should be expected. In addition, the fact that the  $B_4C$  content does not impact the Seebeck coefficient suggests that the carrier mobility may be modified by the  $B_4C$  addition. Therefore, the modification of the electrical resistivity with  $B_4C$  addition may be linked to the carrier mobility changes. The highest values at 800 °C (195  $\mu V/K$ ) are higher than the reported in pure  $Ca_3Co_4O_9$  sintered or textured through spark plasma sintering (170–175  $\mu V/K$ ) [39], but lower than the reported in very dense materials obtained by alternative methods (205  $\mu V/K$ ) [40].

Total  $\kappa$  consists in the addition of two components,  $\kappa = \kappa_l + \kappa_e$ , where  $\kappa_l$  is the lattice thermal conductivity contribution and  $\kappa_e$  is the electronic counterpart.  $\kappa_e$  can be estimated from the Wiedemann-Franz's law [41], which is expressed as  $\kappa_e = L\sigma T$ , where  $L$ , and  $\sigma$  are Lorenz number ( $2.45 \times 10^{-8} V^2/K^2$ ), and electrical conductivity, respectively. The variation with temperature and  $B_4C$  content of the electronic and total thermal conductivity are presented in Fig. 8. When comparing both graphs, it is clear that electronic thermal conductivity is increased when the temperature rises. In contrast, the total thermal conductivity decreases from room temperature to around 600–650 °C induced by the increase of lattice vibrations which enhance phonon scattering. At higher temperatures, the total thermal conductivity increases due to the larger influence of electronic thermal conductivity. Moreover,  $B_4C$  addition leads to a clear decrease of total thermal conductivity, when compared to the pure samples, especially at high temperatures. These results are in agreement with previous works in  $Ca_{3-x}B_xCo_4O_9$  which showed that thermal conductivity is decreased with B-content up to 0.5 [42]. At 800 °C, the minimum total thermal conductivity value determined in 0.25 wt.%  $B_4C$  samples (1.2 W/K m) is about 20 % higher than the lowest measured in these samples (1.0 W/K m at 650 °C). These results are in accordance with the phonon mean free path calculated from  $\kappa_l$ , sound velocity, and heat capacity, as it decreases from the undoped samples (2.5  $\mu m$ ) to the 0.25 wt.%  $B_4C$  ones (1.8  $\mu m$ ), increasing up to 2.2  $\mu m$  for 0.75 wt.%  $B_4C$  samples. These mean free paths are within the range of the reported in the literature [43]. Moreover, these values are comparable to the reported in classically sintered materials (0.9 W/K m with  $\sim 60$  % theoretical density) which show higher amount of porosity [44] than the samples in this work. On the other hand, it is lower than the best values obtained by spark plasma sintering (2.1 W/K m) [45], and much lower

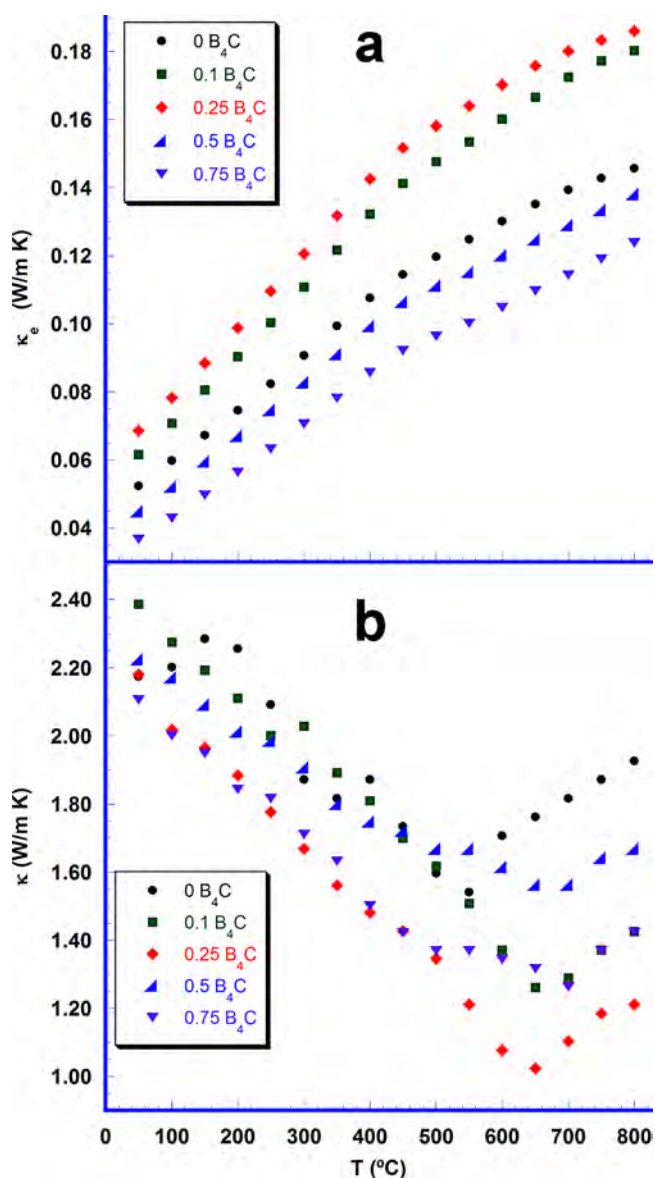


Fig. 8. Evolution of a) Electronic thermal conductivity; and b) Total thermal conductivity, with temperature, as a function of  $B_4C$  content, in  $Ca_3Co_4O_9 + x$  wt.%  $B_4C$  samples.

than the measured in textured materials by hot-uniaxial pressing (2.2, 3, and 4.7 W/K m) [13,44,46]. Other interesting observation is that total thermal conductivity is decreasing with temperature in all samples, reaching a minimum, and then increasing again at higher temperatures. It can be seen that these minima appear at lower temperatures when the  $B_4C$  content is increased. This behaviour can be related to the fact that probably  $\kappa_e$  is typically underestimated in this kind of compounds, as Lorenz number ( $2.45 \cdot 10^{-8} V^2/K^2$ ) used for its calculation is only valid for metallic materials. Consequently, as shown in previous works, it should be calculated as  $L = 1.5 + \exp(-S/116)$ , where  $S$  is the absolute Seebeck coefficient in the maximum [47]. In this work, this expression has not been used, as no  $S$  maximum has been found for any of the prepared samples.

With all the previously discussed data, ZT has been calculated and plotted in Fig. 9. As displayed in the graph, ZT values are increased with temperature in the whole measured temperature range, and also with  $B_4C$  content up to 0.25 wt.%, decreasing for higher additions. The highest value has been measured at 800 °C in 0.25 wt.%  $B_4C$  samples (0.24), which is more than two times higher than the calculated for

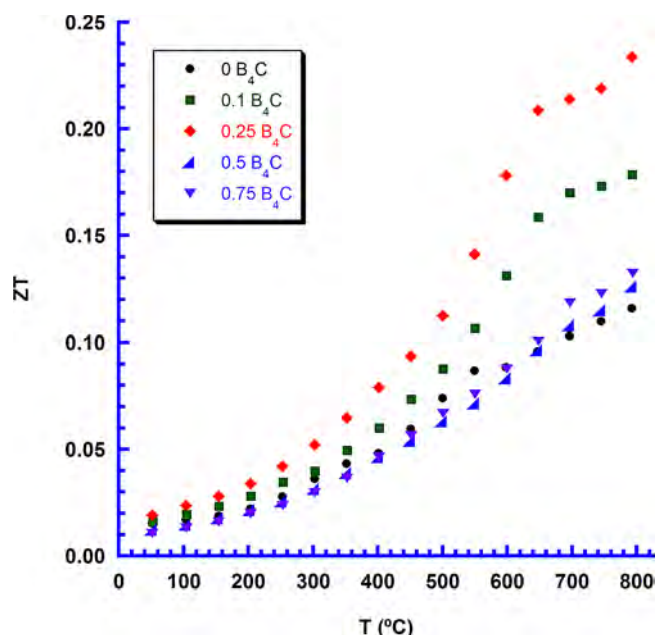


Fig. 9. ZT evolution with temperature, as a function of B<sub>4</sub>C addition in Ca<sub>3</sub>Co<sub>4</sub>O<sub>9</sub> + x wt.% B<sub>4</sub>C samples.

Table 2

Thermal expansion coefficient ( $\alpha$ ) determined in Ca<sub>3</sub>Co<sub>4</sub>O<sub>9</sub> + x wt.% B<sub>4</sub>C samples.

B <sub>4</sub> C content (wt.%)	$\alpha$ (ppm/K)
0	10.32
0.10	9.65
0.25	9.36
0.5	9.56
0.75	9.68

pure ones. Moreover, it is higher than the measured in classically (0.08 [44]), or spark plasma sintered samples (0.15 [45]), and even than the determined in textured samples (0.18, and 0.16 [13,44]). However, this value is lower than the reported one for materials prepared through non-conventional methods (0.35 [15]) or in Ca<sub>3-x</sub>Sr<sub>x</sub>Co<sub>4</sub>O<sub>9</sub> textured materials (0.29 [46]).

Thermal expansion coefficient has been determined in all samples and presented in Table 2. As it can be observed in this table, thermal expansion of pure samples (10.32 ppm/K) is in the range of the reported value for Ca<sub>3</sub>Co<sub>4</sub>O<sub>9</sub> materials (10.6 ppm/K [25]) and lower than the measured in Bi-substituted materials (12.8 ppm/K [25]). On the other hand, B<sub>4</sub>C addition, up to 0.25 wt.%, decreases thermal expansion coefficient, increasing with further additions. The minimum value (9.3 ppm/K) measured in this work corresponds to a decrease of only around 10 % but closer to the one reported for Al<sub>2</sub>O<sub>3</sub> (7.5 ppm/K [48]). This reduction, even if it does not seem to be significant, may reduce the differential thermal expansion between two of the main components of thermoelectric modules, decreasing the internal stresses at working temperatures, and increasing the life span of these devices.

#### 4. Conclusions

Ca<sub>3</sub>Co<sub>4</sub>O<sub>9</sub> + x wt.% B<sub>4</sub>C (x = 0, 0.1, 0.25, 0.5, and 0.75) polycrystalline materials have been prepared through the classical ceramic method. XRD analysis has only identified Ca<sub>3</sub>Co<sub>4</sub>O<sub>9</sub> phase in all samples, independently of the B<sub>4</sub>C content. SEM observations have shown that B<sub>4</sub>C has reacted with oxygen producing liquid B<sub>2</sub>O<sub>3</sub> on its surface, slightly reacting with Ca<sub>3</sub>Co<sub>4</sub>O<sub>9</sub> grains and forming bridges between the grains. These microstructural modifications have been reflected in the

mechanical properties, which were drastically enhanced when compared to the pure samples, despite the slight increase of porosity. Seebeck coefficient has not been affected by B<sub>4</sub>C addition, while electrical resistivity, thermal conductivity and thermal expansion have been decreased, leading to maximum ZT values close to the best reported in the literature, and about two times higher than the measured in pure samples in this work. It is worth to mention that these results have been obtained through a simple and scalable process which can be easily transferred to industry.

#### Declaration of Competing Interest

The authors declare that they have no known competing financial interests or personal relationships that could have appeared to influence the work reported in this paper.

#### Acknowledgements

This study has been funded by the Spanish MINECO-FEDER (Project MAT2017-82183-C3-1-R) and Gobierno de Aragón-FEDER (Research Group T 54-17R). Authors would like to acknowledge the use of Servicio General de Apoyo a la Investigación-SAI, Universidad de Zaragoza.

#### Appendix A. Supplementary data

Supplementary material related to this article can be found, in the online version, at doi:<https://doi.org/10.1016/j.jeurceramsoc.2020.08.024>.

#### References

- [1] G. Mahan, B. Sales, J. Sharp, Thermoelectric materials: new approaches to an old problem, *Phys. Today* 50 (1997) 42–47.
- [2] T.J. Seebeck, Magnetic polarization of metals and minerals, *Abhandlungen der Deutschen Akademie der Wissenschaften zu Berlin* 265 (1822) 1822–1823.
- [3] D.M. Rowe, *Thermoelectrics Handbook: Macro to Nano*, CRC Press, Boca Raton, USA, 2006.
- [4] H. Wang, J. Hwang, M.L. Snedaker, I.-H. Kim, C. Kang, J. Kim, G.D. Stucky, J. Bowers, W. Kim, High thermoelectric performance of a heterogeneous PbTe nanocomposite, *Chem. Mater.* 27 (2015) 944–949.
- [5] X. Wang, H.C. Wang, W.B. Su, F. Mehmood, J.Z. Zhai, T. Wang, T.T. Chen, C.L. Wang, Geometric structural design for lead tellurium thermoelectric power generation application, *Renew. Energy* 141 (2019) 88–95.
- [6] A.A. Yaroshevsky, Abundances of chemical elements in the Earth's crust, *Appl. Geochem.* 44 (2006) 48–55.
- [7] H. Itahara, C. Xia, J. Sugiyama, T. Tani, Fabrication of textured thermoelectric layered cobaltites with various rock salt-type layers by using  $\beta$ -Co(OH)<sub>2</sub> platelets as reactive templates, *J. Mater. Chem.* 14 (2004) 61–66.
- [8] A. Sotelo, Sh. Rasekh, M.A. Torres, P. Bosque, M.A. Madre, J.C. Diez, Effect of synthesis methods on the Ca<sub>3</sub>Co<sub>4</sub>O<sub>9</sub> thermoelectric ceramic performances, *J. Solid State Chem.* 221 (2015) 247–254.
- [9] Z. Shi, J. Xu, J. Zhu, Y. Zhang, T. Gao, M. Qin, H. Sun, G. Dong, F. Gao, Effect of platelet template seeds on microstructure and thermoelectric properties of Ca<sub>3</sub>Co<sub>4</sub>O<sub>9</sub> ceramics, *Ceram. Int.* 45 (2019) 1977–1983.
- [10] Y. Liu, Y. Lin, C.-W. Nan, Z. Shen, Preparation of Ca<sub>3</sub>Co<sub>4</sub>O<sub>9</sub> and improvement of its thermoelectric properties by spark plasma sintering, *J. Am. Ceram. Soc.* 88 (2005) 1337–1340.
- [11] F. Delorme, P. Diaz-Chao, E. Guilmeau, F. Giovannelli, Thermoelectric properties of Ca<sub>3</sub>Co<sub>4</sub>O<sub>9</sub>-Co<sub>3</sub>O<sub>4</sub> composites, *Ceram. Int.* 41 (2015) 10038–10043.
- [12] T. Schulz, J. Toepfer, Thermoelectric properties of Ca<sub>3</sub>Co<sub>4</sub>O<sub>9</sub> ceramics prepared by an alternative pressure-less sintering/annealing method, *J. Alloys Compd.* 659 (2016) 122–126.
- [13] H. Wang, X. Sun, X. Yan, D. Huo, X. Li, J.-G. Li, X. Ding, Fabrication and thermoelectric properties of highly textured Ca<sub>9</sub>Co<sub>12</sub>O<sub>28</sub> ceramic, *J. Alloys Compd.* 582 (2014) 294–298.
- [14] S. Lemonnier, C. Goupil, J. Noudem, Four-leg Ca<sub>0.95</sub>Sm<sub>0.05</sub>MnO<sub>3</sub> unileg thermoelectric device, *J. Appl. Phys.* 104 (2008) 014505.
- [15] A. Sotelo, F.M. Costa, N.M. Ferreira, A. Kovalevsky, M.C. Ferro, V.S. Amaral, J.S. Amaral, Sh. Rasekh, M.A. Torres, M.A. Madre, J.C. Diez, Tailoring Ca<sub>3</sub>Co<sub>4</sub>O<sub>9</sub> microstructure and performances using a transient liquid phase sintering additive, *J. Eur. Ceram. Soc.* 36 (2016) 1025–1032.
- [16] Y.C. Liou, W.C. Tsai, W.Y. Lin, U.R. Lee, Synthesis of Ca<sub>3</sub>Co<sub>4</sub>O<sub>9</sub> and CuAlO<sub>2</sub> ceramics of the thermoelectric application using a reaction-sintering process, *J. Aust. Ceram. Soc.* 44 (2008) 17–22.

- [17] W.M. Haynes, T.J. Bruno, D.R. Lide, CRC Handbook of Chemistry and Physics, CRC press, Florida, USA, 2016.
- [18] E. Woermann, A. Muan, Phase equilibria in the system CaO-cobalt oxide in air, *J. Inorg. Nucl. Chem.* 32 (1970) 1455–1459.
- [19] JCPDS 21-0139.
- [20] G.C. Karakaya, B. Ozelcik, M.A. Torres, M.A. Madre, A. Sotelo, Effect of Na-doping on thermoelectric and magnetic performances of textured  $\text{Bi}_2\text{Sr}_2\text{Co}_2\text{O}_y$  ceramics, *J. Eur. Ceram. Soc.* 38 (2018) 515–520.
- [21] JPDF card #35-0798.
- [22] F. Delorme, C.F. Martin, P. Marudhachalam, G. Guzman, D.O. Ovono, O. Fraboulet, Synthesis of thermoelectric  $\text{Ca}_3\text{Co}_4\text{O}_9$  ceramics with high ZT values from a  $\text{Co}^{\text{II}}$   $\text{Co}^{\text{III}}$ -Layered Double Hydroxide precursor, *Mater. Res. Bull.* 47 (2012) 3287–3291.
- [23] A.I. Klyndyuk, I.V. Matsukevich, Structure, and Properties of  $\text{Ca}_3\text{Co}_{3.85}\text{M}_0.15\text{O}_9+\delta$  ( $\text{M} = \text{Ti-Zn, Mo, W, Pb, Bi}$ ) Layered Thermoelectrics, *Inorg. Mater.* 51 (2015) 944–950.
- [24] Z. Shi, F. Gao, J. Xu, J. Zhu, Y. Zhang, T. Gao, M. Qin, M. Reece, H. Yan, Two-step processing of thermoelectric  $(\text{Ca}_{0.9}\text{Ag}_{0.1})_3\text{Co}_4\text{O}_9$ /nano-sized Ag composites with high ZT, *J. Eur. Ceram. Soc.* 39 (2019) 3088–3093.
- [25] I.V. Matsukevich, A.I. Klyndyuk, E.A. Tugova, A.N. Kovalenko, A.A. Marova, N.S. Krasutskaya, Thermoelectric Properties of  $\text{Ca}_{3-x}\text{Bi}_x\text{Co}_4\text{O}_9+\delta$  ( $0.0 \leq x \leq 1.5$ ) Ceramics, *Inorg. Mater.* 52 (2016) 593–599.
- [26] D. Sedmidubsky, V. Jakes, O. Jankovsky, J. Leitner, Z. Sofer, J. Hejtmanek, Phase equilibria in Ca–Co–O system, *J. Solid State Chem.* 194 (2012) 199–205.
- [27] L.M. Litz, R.A. Mercuri, Oxidation of boron carbide by air, water and air-water mixtures at elevated temperatures, *J. Electrochem. Soc.* 110 (1963) 921–925.
- [28] E.H.P. Cordfunke, R.J.M. Konings, Thermochemical Data for Reactor Materials and Fission Products, Elsevier Science Publishers, North-Holland, 1990.
- [29] L. Belovsky, Heat release from  $\text{B}_4\text{C}$  oxidation in steam and air, IAEA-TECDOC-921, International Atomic Energy Agency (IAEA), 1996, pp. 49–61.
- [30] H. Yu, Q. Chen, Z.P. Jin, Thermodynamic assessment of the  $\text{CaOB}_2\text{O}_3$  system, *Calphad* 23 (1999) 101–111.
- [31] I.N.K. Belyaev, K Voprosu o diagramme sostoyaniya sistemy  $\text{CoO-B}_2\text{O}_3$ , *Zh. Fiz. Khim.* 30 (1956) 1419.
- [32] D. Kenfaui, M. Gomina, D. Chateigner, J.G. Noudem, Mechanical properties of  $\text{Ca}_3\text{Co}_4\text{O}_9$  bulk oxides intended to be used in thermoelectric generators, *Ceram. Int.* 40 (2014) 10237–10246.
- [33] R.W. Rice, Mechanical Properties of Ceramics and Composites, Marcel Dekker, 2000.
- [34] R.W. Rice, The compressive strength of ceramics, materials science research, *Ceram. Severe Environ.* 5 (1971) Plenum.
- [35] Y.H. Lin, High-temperature electrical transport behaviors in textured  $\text{Ca}_3\text{Co}_4\text{O}_9$ -based polycrystalline ceramics, *Appl. Phys. Lett.* 94 (2009) 072107.
- [36] S. Pinitsoontorn, N. Lerssongkram, N. Keawprak, V. Amornkitbamrung, Thermoelectric properties of transition metals-doped  $\text{Ca}_3\text{Co}_{3.8}\text{M}_{0.2}\text{O}_9+\delta$  ( $\text{M} = \text{Co, Cr, Fe, Ni, Cu}$  and  $\text{Zn}$ ), *J. Mater. Sci. Mater. Electron.* 23 (2012) 1050–1056.
- [37] Sh. Rasekh, M.A. Torres, G. Constantinescu, M.A. Madre, J.C. Diez, A. Sotelo, Effect of Cu by Co substitution on  $\text{Ca}_3\text{Co}_4\text{O}_9$  thermoelectric ceramics, *J. Mater. Sci. Mater. Electron.* 24 (2013) 2309–2314.
- [38] L. Zhang, T.T. Tan, S. Li, The effects of composition deviations on the micro-structure and thermoelectric performance of  $\text{Ca}_3\text{Co}_4\text{O}_9$  thin film, *J. Mater. Sci. Mater. Electron.* 29 (2018) 13321–13327.
- [39] D. Kenfaui, G. Bonnefont, D. Chateigner, G. Fantozzi, M. Gomina, J.G. Noudem,  $\text{Ca}_3\text{Co}_4\text{O}_9$  ceramics consolidated by SPS process: Optimisation of mechanical and thermoelectric properties, *Mater. Res. Bull.* 45 (2010) 1240–1249.
- [40] M.A. Madre, F.M. Costa, N.M. Ferreira, A. Sotelo, M.A. Torres, G. Constantinescu, Sh. Rasekh, J.C. Diez, Preparation of high-performance  $\text{Ca}_3\text{Co}_4\text{O}_9$  thermoelectric ceramics produced by a new two-step method, *J. Eur. Ceram. Soc.* 33 (2013) 1747–1754.
- [41] M.E. Fine, N. Hsieh, Wiedermann-Franz-Lorenz relation in highly electronic-conducting oxides, *J. Am. Ceram. Soc.* 57 (1974) 502–503.
- [42] S. Altin, A. Bayri, S. Demirel, M.A. Aksan, Thermal conductivity and magnetic properties of the B substituted  $\text{Ca}_3\text{Co}_4\text{O}_9$ , *Curr. Appl. Phys.* 14 (2014) 590–595.
- [43] K.T. Regner, D.P. Sellan, Z. Su, C.H. Amon, A.J.H. McGaughey, J.A. Malen, Broadband phonon mean free path contributions to thermal conductivity measured using frequency domain thermoreflectance, *Nature Commun.* 4 (2013) 1640.
- [44] D. Kenfaui, B. Lenoir, D. Chateigner, B. Ouladidaf, M. Gomina, J.G. Noudem, Development of multilayer textured  $\text{Ca}_3\text{Co}_4\text{O}_9$  materials for thermoelectric generators: Influence of the anisotropy on the transport properties, *J. Eur. Ceram. Soc.* 32 (2012) 2405–2414.
- [45] R. Tian, T. Zhang, D. Chu, R. Donelson, L. Tao, S. Li, Enhancement of high temperature thermoelectric performance in Bi, Fe co-doped layered oxide-based material  $\text{Ca}_3\text{Co}_4\text{O}_9+\delta$ , *J. Alloys Compds.* 615 (2014) 311–315.
- [46] M.A. Torres, F.M. Costa, D. Flahaut, K. Touati, Sh. Rasekh, N.M. Ferreira, J. Allouche, M. Depriester, M.A. Madre, A.V. Kovalevsky, J.C. Diez, A. Sotelo, Significant enhancement of the thermoelectric performance in  $\text{Ca}_3\text{Co}_4\text{O}_9$  thermoelectric materials through combined strontium substitution and hot pressing process, *J. Eur. Ceram. Soc.* 39 (2019) 1186–1192.
- [47] J. Prado-Gonjal, F. Serrano-Sánchez, N.M. Nemes, O.J. Dura, J.L. Martínez, M.T. Fernández-Díaz, F. Fauth, J.A. Alonso, Extra-low thermal conductivity in unfilled  $\text{CoSb}_3\delta$  skutterudite synthesized under high pressure conditions, *Appl. Phys. Lett.* 111 (2017) 083902.
- [48] C.J. Engberg, E.H. Zehms, Thermal expansion of  $\text{Al}_2\text{O}_3$ ,  $\text{BeO}$ ,  $\text{MgO}$ ,  $\text{B}_4\text{C}$ ,  $\text{SiC}$ , and  $\text{TiC}$  above  $1000^\circ\text{C}$ , *J. Am. Ceram. Soc.* 42 (1959) 300–305.